An end-to-end instrument model for the proposed E-ELT instrument METIS

E. Schmalzl*[a], J. Meisner[a], L. Venema[b], S. Kendrew[c] B. Brandl[a], J. Blommaert[d], A. Glasse[e], R. Lenzen[c], M. Meyer[f], F. Molster[g,a], E. Pantin[h],

[a]Leiden Observatory, University of Leiden, PO Box 9513, 2300 RA Leiden, Netherlands;
[b]ASTRON, Oude Hoogeveensedijk 4, 7991 PD Dwingeloo, The Netherlands;
[c]Max-Planck-Institut für Astronomie, Königstuhl 17, 69117 Heidelberg, Germany;
[d]Katholieke Universiteit Leuven, Institute of Astronomy, Celestijnenlaan 200D Bus 2401, 3001 Leuven, Belgium;
[e]UK Astronomy Technology Center, Royal Observatory of Edinburgh, Blackford Hill, Edinburgh EH9 3HJ, United Kingdom;
[f]ETH Zürich, Institute for Astronomy, Wolfgang-Pauli-Strasse 27, 8093 Zürich, Switzerland;
[g]DutchSpace, P.O. Box 32070, 2303 DB Leiden, The Netherlands;
[h]CEA Saclay, Gif-sur-Yvette, 91191 Cedex, France

ABSTRACT

The optimal performance of an instrument relies critically on accurate performance estimates during its design phase. They need to be modeled to give the science and engineering teams a preview of the performance of the instrument, to guide the design process, to prove the capabilities of the instrument and to prepare science ready software tools before the instrument is operational. METIS, the Mid-infrared E-ELT Imager, is an instrument concept for the E-ELT that covers the thermal infrared wavelengths from $2.9 - 14\mu m$ (L, M and N band). It contains a diffraction limited imager and an integral field high resolution spectrograph. The instrument consists of two independent units, the imager and the spectrograph, and is entirely encased in a cryostat to maintain the stable low temperatures required for good performance at mid-infrared wavelengths. METIS was identified in the instrument roadmap as the third instrument for the E-ELT, after two first light instruments. Because in the mid-infrared the Earth's atmosphere and the telescope mirrors radiate and produce a very high thermal background, it is crucial to develop techniques and mechanisms to measure and reduce this background, to achieve the desired performance of an E-ELT. To demonstrate the capabilities of METIS, years before the actual instrument is built and can be tested, we are developing an end-to-end instrument model, which will simulate the full capacity of METIS. The structure of the model and first results of the performance evaluation are shown.

Keywords: E-ELT, METIS, infrared instrumentation, instrument model, sensitivity, performance

1. THE METIS INSTRUMENT

METIS[1] is the only mid-infrared instrument concept for the 40 m-class European Extremely Large Telescope (E-ELT)[2] that covers the thermal infrared wavelengths range from $2.9 - 14\mu m$, covering the L, M and N bands. It is expected to start operations in 2020 as the third instrument after the two first light instruments MICADO, a diffraction limited near-infrared camera,[3] and HARMONI, a wideband, integral-field spectrograph.[4] METIS is being designed and built by a consortium of NOVA (representing Leiden Observatory and ASTRON, Netherlands), the Max Planck Institute for Astronomy (MPIA, Germany), UK Astronomy Technology Center (UKATC, UK), Katholieke Universiteit Leuven (Belgium), CEA Saclay (France) and ETH Zürich (Switzerland).

*mail to: E. Schmalzl, meyer@strw.leidenuniv.nl

1.1 Mid-infrared Science with the E-ELT and METIS

Generally, mid-IR astronomy focuses mainly on objects that are very dusty or dust-obscured, intrinsically cool or significantly redshifted by the cosmic expansion. Furthermore, the mid-IR wavelength range is extremely rich in spectral diagnostics, complementary to those found at other wavelengths: emission and absorption lines of virtually all molecules, numerous atoms and ions, and unique solid state features. The METIS science team identified five main science drivers, for which METIS is expected to produce breakthrough science:

- Proto-planetary disks and the formation of planets
- Physical and chemical properties of exoplanets
- Formation and history of the solar system
- The growth of supermassive black holes
- Morphologies and dynamics of high-redshift galaxies

and many more.

METIS will allow unique observations of a wide range of astrophysical targets, providing complementarity with other facilities such as JWST and the Atacama Large Millimeter Array (ALMA). Because of Earth's atmosphere, which absorbs infrared wavelengths as well as radiates a strong and variable thermal background, observing in the mid-infrared is very difficult and challenging. But thanks to the huge collecting area of the E-ELT, METIS will offer unrivaled spatial and spectral resolution, far surpassing that of contemporary space-based instruments such as JWST/MIRI. The study of compact objects in the near and distant universe at the highest spatial and spectral resolutions, is one of the unique strengths of METIS.
The E-ELT will create entirely new perspectives in optical/IR astronomy. Taking advantage of the supreme spatial resolution from a 40-m-class aperture, METIS will open up a huge discovery space at mid-infrared wavelengths - a thus far relatively unexplored region at the highest resolution. For further details on the METIS and its science cases see also Brandl et al.[5] in these proceedings (paper 8446-57).

1.2 The instrument design

METIS will work in the mid-infrared wavelength regime and the basic design of the instrument includes the following observing modes:

- Diffraction limited imaging in the L ($2.9 - 4.2\mu m$), M ($4.5 - 5.5\mu m$) and N bands ($8.0 - 14.0\mu m$) with a field of view of $18'' \times 18''$
- Coronographic imaging in the L and N bands
- Low resolution slit spectroscopy in L, M and N bands, with a resolution $R \sim 900 - 5000$
- Polarimetry in N band for imaging and low resolution spectroscopy
- IFU-fed high-resolution spectrograph in L and M bands with a field of view of $0.4'' \times 1.5''$ and a resolution $R \sim 100000$

The instrument consists of two separated units, one for the imager, including the coronograph, polarimeter and low-resolution spectrograph and one for the high-resolution integral field spectrograph. An optical overview of the instrument is shown in Fig.1.

The instrument will be entirely encased in a spherical cryostat to maintain the stable low temperatures necessary for a good detector performance and to reduce the thermal background radiation originating inside the

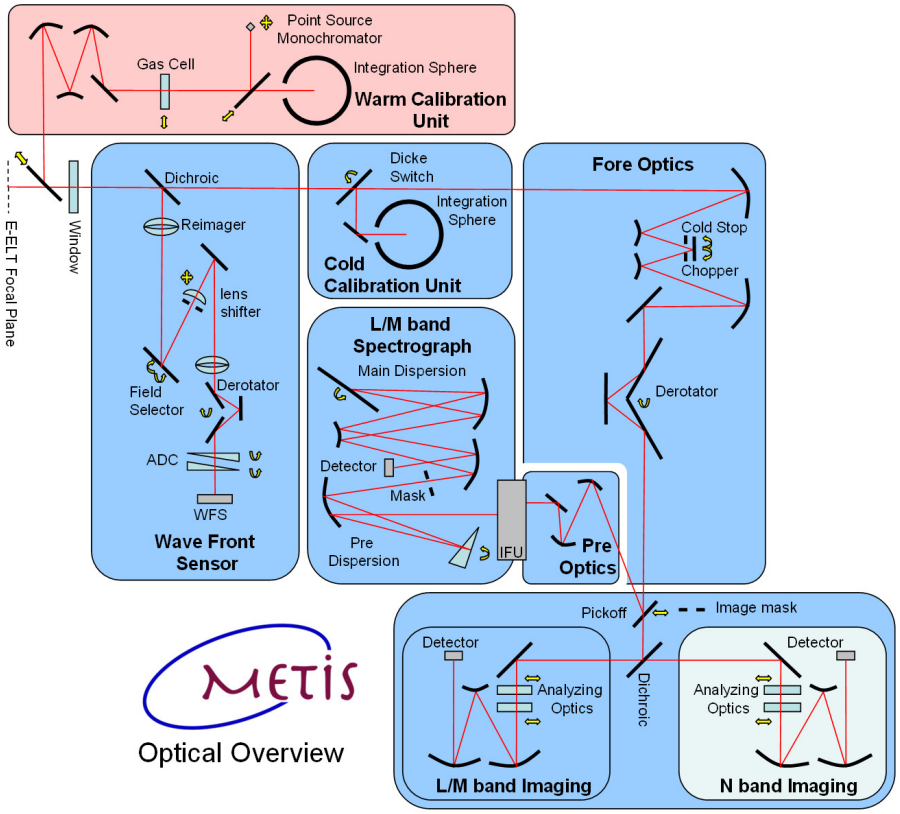

Figure 1. Conceptual optical overview of METIS

instrument, which is required for a good performance in the mid-infrared wavelengths regime.

To achieve diffraction limited performance over the full wavelength range, METIS will use adaptive optics (AO) correction to compensate for atmospheric turbulence. The 2.6 m M4 mirror of the E-ELT's main optical path will provide AO correction (see[2] for more details on the design of the E-ELT), while the sensing of the wavefront will be carried out internally in METIS. For most of the targets of METIS a single-conjugated natural guide star sensing will be used, as those targets are compact and bright. For the extended and/or faint targets laser guide star tomography (LTAO) will be used at a later stage of the E-ELT development and implementation.

The calibration and subtraction of the thermal background originating from the sky, telescope and instrument will be performed by an internal chopping mechanism, located in the fore optics and a unique Dicke-switch in the cold calibration unit (see Fig. 1). The Dicke-switch is a fast tilting mirror which rapidly switches the input beam of the following imager and spectroscopic modules between the science beam and the one coming from the internal cold, and on a constant temperature, calibration unit. Detector related noise sources, such as gain instability, can be measured and later corrected in this way. A designated analysis of the performance of the Dicke-Switch is carried out additionally and the findings resulting from this analysis will be implemented in the here described end-to-end model at a later stage.

2. THE SIMULATION PROGRAM

Given the complexity of thermal radiation transfer along the many optical components of telescope and instrument, the need for an instrument simulator is obvious. To assess the instrument performance, guide the design

process, prove capabilities of the instrument and prepare science ready software tools, years before the instrument is ready, we are developing an end-to-end model of the whole instrument plus telescope and atmosphere. The simulation program runs each essential aspect of this model in a greater or lesser degree of detail in order to generate an output that is expected to resemble the output data stream that the instrument would produce. Although the software package is far from complete[†] it is already capable of generating detector data in straight imaging mode (modules implementing the spectroscopic modes of the instrument have yet to be written) based on an assumed source image on the sky, the PSF of the telescope and instrument's optics, the thermal background from the atmosphere and warm optics, the throughput of the atmosphere and each intervening optical element, and the characteristics of the detector chip. In each case the relevant modelling is specified as a function of wavelength, using some specified discretization of the wavelength scale which can be specified from very low to arbitrarily high spectral resolution, depending on the requirements for a particular simulation problem. Likewise, image information at various stages of processing may be specified to be of a lower or higher resolution, but in this respect the final image is of course required to be represented according to the pixel layout of the detector chip(s) simulated.

The simulator has so far been implemented in the interactive language IDL, with the goal of a translation to Python at a later stage, as in a future version some computationally intensive routines may be implemented in C/C++, for instance, and called by the program, which can be realized in a simpler way in Python. Input and output data will (mainly) employ FITS[6] files to describe the images and detector outputs, along with plans to enhance the data description using embedded FITS binary tables to encode the spectral aspects of the simulated input images. In the following sections we describe the architecture of the simulator and its internal data representation.

2.1 Input parameters

The input parameters governing the simulator, intended to as closely as possible represent the characteristics of the E-ELT and METIS hardware, are taken from a variety of sources. Specifications of the E-ELT telescope parameters are taken from the latest design report, as of 2011[2] , site information from the TMT site study[7] and instrumental parameters from the final design of METIS as of November 2009, see also[8] for more details on the input parameters. Detector specifications are taken from the manufacturer where available or from newest analysis of existing instruments, such as VISIR. Atmospheric transmission and emission models are available which can be imported into the simulator at any required spectral resolution. The applied input parameters for the telescope and detector are summarized in Tab. 1.

For a particular simulation, a file containing keywords and values will be input which will effectively place the METIS hardware in one or another operating mode and may describe the pointing of the telescope toward an astronomical target. An assumed underlying image of the observed field can be supplied along with spectral information in order to define an underlying "input image" in one of the forms described below which are used by the imaging track of the simulator.

Parameters supplied in the setup file will determine the precision with which various aspects of the E-ELT/METIS hardware are simulated. For instance, one may choose the spatial resolution, spectral resolution, and update rates of different stages of the simulator in order to attack a particular problem. Relaxing the requirements of some aspects of the simulation thereby saves computing time which can better be spent on a more refined simulation of the functions pertinent to addressing particular aspects of the system's performance. Operating parameters such as the detector readout rate or selection of spectral filters can be explored in order to determine their effect on the resulting simulator output. In this way, not only can the feasibility of a proposed observation be verified, but the performance of that observation can be optimized in simulation long before it is carried out in practice.

2.2 Image and spectral representation

The system is required to be capable of simulating in detail images at a rather high spatial resolution and spectral features at a high spectral resolution. On the other hand, certain simulations will be required to be

[†]Indeed it might never be fully "complete" inasmuch as it is defined by a framework to which one can add or substitute modules in order to implement new functions or implement existing functions differently or with improved precision.

Table 1. Input parameters currently used for the performance simulation.

Telescope parameters	**Value**	
Fully enclosed outer diameter M1	37 m	
Fully enclosed inner diameter M1	11.1 m	
Obscured area due to spiders	3.3% of primary area	
Area of primary aperture (M1)	1004.0 m^2	
Area of primary aperture, masked	937.5 m^2	
Nominal mirror reflectivity	98%	
Numbers of Mirrors	5	
Net primary mirror emissivity[a]	15%	
Ambient temperature (median)	280.65 K	
Detector parameters	**L-M band (Hawaii II)**	**N band (Aquarius)**
size [pixel]	2048×2048	1024×1024
Read-noise, rms. [e^-/frame/pixel]	20	2000
Dark current [e^-/s/pixel]	0.5	< 2000
Well depth [e^-/pixel]	130000	1.4×10^7
Pixel size [μ m]	18×18	30×30
Detector quantum efficiency	0.84	0.6

[a] The emissivity is calculated as the combined emissivity from the mirrors, the spacing between the primary mirror segments and the spiders.

simulated with good temporal resolution (in order to model dynamic aspects of an observation such as image jitter), involving many repeated calculations over a simulated time series. The simulator architecture has been devised in order to accommodate any arbitrary level of spatial, spectral, and/or temporal resolution. But for reasons of computational practicality, all of these capabilities are not implemented simultaneously beyond what is required to address a particular problem in which, typically, either the spatial, spectral, or temporal aspect is of prime significance.

The temporal aspect of the simulator is governed by the outer level of programming which calls the functional blocks which actually act on images and spectra. Different update rates can thereby be specified for different aspects of the simulation, so that a stage in the processing where temporal evolution of the data is unimportant or uninteresting can be only infrequently run; in many situations a stage need only be run a single time. When a stage has been run, the data product that it has produced will receive a simulated time stamp, and all subsequent stages using its result will be required to be run using their new inputs. But the opposite is not true. So for instance, in simulations concentrating on the detector aspect of the instrument, one might run all of the stages shown in Fig. 2 a single time, presenting the same optical illumination to the detector module which can then be run thousands or millions of times using that one unchanging input. This level of flexibility saves an enormous amount of computation compared to repeated, but pointless, execution of the entire data path.

Likewise, a great deal of flexibility has been built into the image and spectral representations in order to again avoid extremely slow computation. Moreover, the memory storage requirements of these data could become an issue in itself. Although IDL has no formal limitations on the size of data structures stored in memory, very large amounts of data involved in a computation will in fact be diverted into the computers swap space (virtual memory actually residing on disk), in which case computations involving those data become *much* slower, as most of the computer time is hogged by the operating system in order to swap physical and virtual memory even during a single computation. For all these reasons, steps have been taken to reduce the storage requirements to describe otherwise allowable data representations required to address a particular simulation problem. In the following we describe the three possible representations for simulated images and their spectra.

2.2.1 Imagecube mode

The most straight forward representation of image data is representation as an *imagecube*, a three dimensional array including the two spatial (image) directions and the third dimension representing wavelength.

This mode of representation, as well as the other modes described below, rely first on a "wavelength setup" wherein the spectral range of interest is divided up into **M** wavelength bins, each represented by a center wavelength and a bandwidth, such that the bins are contiguous over the spectral ranges of interest with neither overlap nor underlap. The spacing between the wavelengths (and thus the bandwidths of the bins) need neither be fixed or in any way regular. So, for instance, a simulation which is probing the capabilities of one of the spectroscopic modes may have a high density of wavelength bins around the spectral lines of interest, while still representing the entire spectrum at a much lower resolution in order that simultaneous imaging of the continuum can be simulated. Whatever wavelength setup is adopted for the underlying input image to the simulator applies to all intermediate data passing through the simulator, and is unchanged for the duration of that simulation.

In imagecube mode, the underlying image of a field on the sky of up to 17 $arcsec^2$ (but much smaller when possible) is represented spatially in a **J** by **K** pixel image, with **M** such image planes each representing the flux contained in each of the **M** wavelength bins as described above. Since there is no limit on the spatial or spectral resolution that a user may demand, the requirement to store and process data objects consisting of $\mathbf{J} \times \mathbf{K} \times \mathbf{M}$ floating point numbers can in some cases be overwhelming. In these cases, imagecube mode is not a reasonable option. In many other cases the storage requirement would not be a great burden, but the data would still be quite well described using one of the other modes, thereby increasing the computational efficiency of the simulation.

However datacube representation remains an option given its simplicity and generality. Often either the required spectral resolution is limited (so that **M** can be a rather small number), only low spatial resolution is required (thus allowing for a large pixel size), the area on the sky is limited (such as simulations destined for the integral field spectrograph), or the area on the sky is narrow in one dimension (such as simulations for the long slit spectrographs). In such cases the storage requirement of $\mathbf{J} \times \mathbf{K} \times \mathbf{M}$ can be easily accommodated.

2.2.2 Monochrome mode

In *monochrome mode*, there is but a single image plane, and a single spectrum attached to that image. In other words, the image is considered to be of a particular color, but that "color" can be specified with a high degree of spectral resolution if required. After all, the storage requirement for the single image plus single spectrum is now only $\mathbf{J} \times \mathbf{K} + \mathbf{M}$, so any of these dimensions could be quite large. While a monochrome image of this sort could never accurately describe an actual field on the sky, it may be entirely sufficient to handle many practical simulations. For instance, spectroscopy on a single star may only require describing the image of that star (generally being the PSF of the instrument for otherwise unresolved stars) along with an assumed spectrum for the whole star which could be specified using a very high resolution (large **M**) wavelength setup. Or another simulation may only be concerned with imaging aspects of the instrument regardless of specific spectral features inherent in the image or optical transmission. In these cases monochrome mode may be quite adequate.

2.2.3 N-chrome mode

The third mode for image (and spectrum) representation is more powerful than monochrome mode, but generally more efficient than datacube mode. In *N-chrome mode*, the image is organized spatially as $\mathbf{J} \times \mathbf{K}$ pixels, but there are **N** such image planes, each with its own (possibly high resolution) spectrum. This mode, again, has a greatly reduced storage requirement in comparison with imagecube mode, but may be ideal for describing many underlying models which include various "colors," each of which can be described in arbitrarily high spectral detail.

One simple-minded example might be a field containing 20 stars of interest which will be observed spectroscopically. Then one could just assign one of the $\mathbf{N}=20$ image planes to each star, and each star would appear on only one of those image planes. But each image plane has associated with it a (possibly) high resolution spectrum, in this case each corresponding to the model spectrum for one star. Or in another example, one may want to model emission from dust of various temperatures. Again, one could simplistically assign dust of 1000° K to one "color," dust of 1100° K to another color, and so on, with a spectrum attached to each plane describing dust emission at that temperature. Now, having to assign every dust temperature to the nearest 100° K may seem rather coarse, so one might choose to use more image planes (larger **N**) for a finer gradation between temperatures; the storage requirements for $\mathbf{J} \times \mathbf{K} \times \mathbf{N}$ image pixels (plus $\mathbf{N} \times \mathbf{M}$ spectral points) would still be reasonable. More

intelligently, however, one might interpolate dust temperatures in between those defined for the image planes and assign part of the flux to one temperature and part to the next temperature image plane. After all, the represented image at one spatial pixel j, k consists of the sum of the pixels in all image planes j, k, n_1, j, k, n_2, j, k, n_3 ... each with its own **M** point spectrum. One can appreciate that the "N-chrome" representation is still a very powerful description for most models, even with high spatial and spectral resolution, with greatly reduced storage requirements compared to the $\mathbf{J} \times \mathbf{K} \times \mathbf{M}$ elements that full imagecube mode would require.

Although we have described "three representations" for spectral-image data, the reader may have noticed that monochrome mode is merrily a special case of N-chrome mode where **N**=1. Consequently there is no special programming required for monochrome mode above that of N-chrome mode. And, it might be added, that the handling of imagecube data also differs very little. In fact, imagecube mode could be conceptually viewed as a special case of N-chrome data where **N**=**M** and each of the **N** spectra consists but of one non-zero element. However the internal representation of imagecube data doesn't require an array of such trivial spectral mappings, as the mapping from image plane **M** to wavelength bin **M** is simply coded.

2.3 Program structure

The simulator is composed of five basic functional blocks, each of which is composed of one or more modules (routines with a well-defined input, output, and range of behaviours) which together follow the radiation representing the simulated image of an object on the sky, along with thermal radiation especially from the atmosphere and warm optical elements, all the way to the production of photoelectrons in the detector which are presented to the readout electronics and digitized to produce the expected data product supplied by the METIS hardware. This output data would be available as a test input to data reduction software written for METIS when that becomes available; at present those data are only handled using simple routines included within the simulator itself, notably in order to stack detector images for inspection.

In addition to support and control aspects of the software, the simulator contains functional blocks which implement the following functionalities required to process a simulated optical signal from an astronomical target as seen from above the atmosphere, to the point of producing the output of the detectors.

- The *image track* follows the underlying spatial image through the atmosphere, telescope, and METIS optics up to the camera or spectrometer.
- The *throughput track* calculates the effect that those optical components have in reducing the (spectral) brightness of that image independent of image position.
- The *background track* processes the same series of optical components addressed by the throughput track, but models the emission from these elements due to their temperature (the elements that are not in the cryostat) to determine the net background emission that is incident at the entrance of the modelled camera or spectrometer.
- The *camera or spectrometer function* is implemented for each of the instrument modes in order to map photons outputted according to the imaging, throughput, and background tracks onto one or more of the three detector arrays.
- The *detector function* receives that photon flux and produces not only the intended photocurrent, but detection noise and any detector artifacts (such as non-linearity, saturation, nonuniform pixel gain or dark level, etc.) that we choose to model.

These five blocks are each identified in the simplified block diagram of the simulator architecture shown in Fig. 2, and are further described in the following sections.

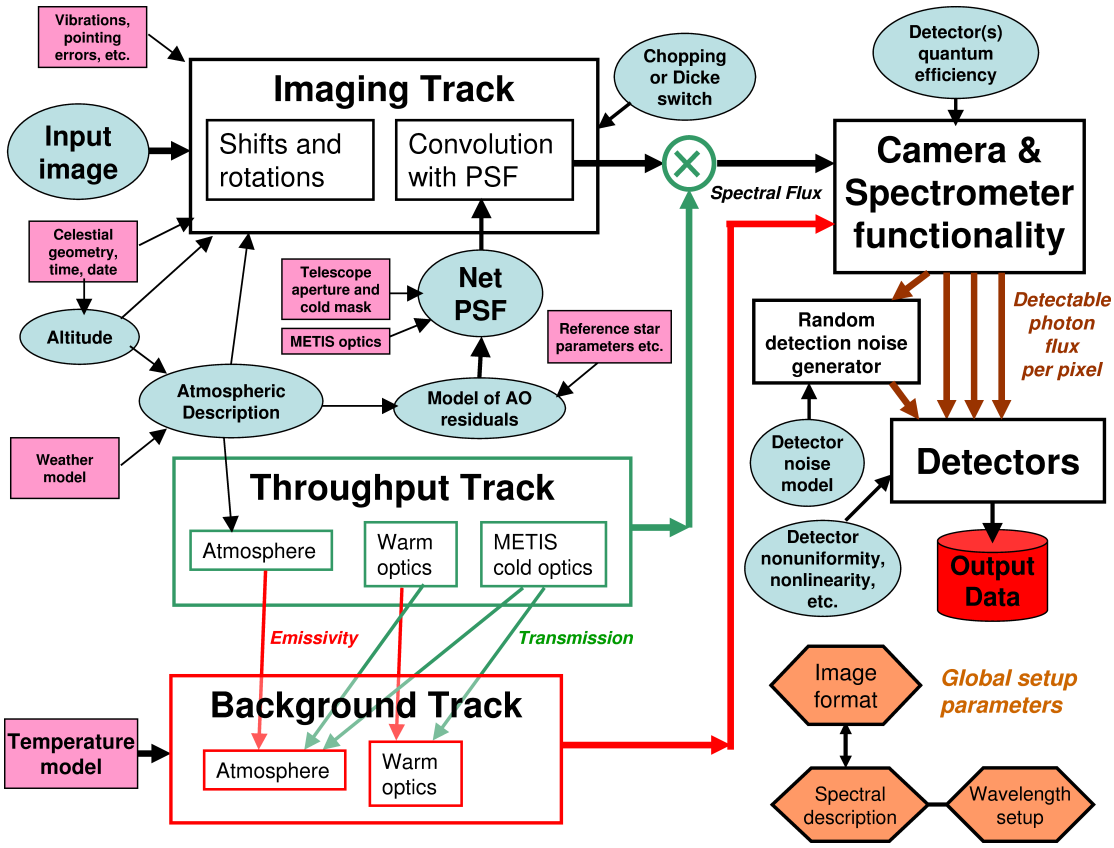

Figure 2. Simplified block diagram of the simulator architecture.

2.3.1 Imaging Track

The imaging track follows the spatial representation of the incoming source radiation as that radiation either focuses to a real image, or in most cases as a virtual image (in other words, the image that would be formed at focus if an imaginary lens were inserted at that point in the optical train). The image description at each point is accompanied by the spectral information according to one of the image representations described above, but this spectral information is not acted upon by the imaging track; that is done by the throughput track (sect. 2.3.2). However in imagecube mode and in N-chrome mode, there are some modules within the imaging track which operate selectively according to the effective wavelength (or specific spectrum) attached to each of the **N** image planes. Other modules are simply geometrical and operate on all image planes identically.

Below are a list of modules, in order, contemplated for the imaging track which describe each aspect of the model from the assumed astronomical source to the input position of the camera and/or spectrometer functionality (where METIS happens to form a real image) but not including the IFU pickoff or the L-M to N band dichroic mirror which are rather grouped with the camera functionality block. Note that this list is overly complete, in that it addresses more details of the image transfer than most simulation jobs would ever require. In normal practice a number of these operations could be ignored or abbreviated. For instance, in many simulations differential atmospheric refraction and the non-radially symmetric aspect of the telescope PSF may be of no concern. In such a simulation then, the image rotations modeling the celestial sphere and the telescope's pointing on the sky and internal geometry, and the opposite rotation supplied by the image rotator of METIS, can all be dispensed with since they cancel each other out.

- Translation and rotation from the source image described on the celestial sphere (in RA and DEC coordinates) to the apparent position on the sky seen from the E-ELT (in alt-az coordinates) centered around

the nominal pointing (optical axis) of the telescope.

- Differential refraction by the atmosphere, weakly a function of wavelength so that the various image planes (colors) are shifted vertically by slightly different amounts.
- Convolution of the image with the PSF of the telescope (possibly including the overlapping mask, actually implemented at the cold stop of the METIS fore optics) as well as the effect of residual atmospheric turbulence not corrected by the AO system. Since the PSF is a function of wavelength, again each image plane is convolved separately with a somewhat different function.
- A spatial shift in the image (non-chromatic) can optionally be implemented in order to model telescope vibrations (ones which are not tracked by the AO and tip-tilt systems) or pointing errors.
- Rotation by the telescope's optics to the Nasmyth coordinate system (horizontal and vertical) at the point just before the light enters the METIS cryostat.
- When the warm calibration unit is optionally directed into the METIS optics, the astronomical image would be destroyed at this point and replaced by an image (and spectrum) determined by the warm calibration unit operating in one or another mode.
- When the Dicke switch (cold calibration unit) is switched in, the on-sky image is destroyed (and the background radically changed) through the change of an element in the throughput structure as mentioned in sect. 2.3.2.
- The chopping mirror may be modelled as an image shift whose magnitude is dependent on the modeled tilt of the chopping mirror at that instant. The chopping mirror is conjugate to the pupil (see Fig. 1).
- The image (de-)rotator inside METIS is modeled as an image rotation according to the commanded position of those three reflecting surfaces (see Fig. 1).

The above modules are built out of a few different elementary functions applied as required. One such function is that of convolution with a point spread function (PSF) which had either been precomputed (in the case of a fixed PSF) or may have been newly recomputed for simulations in which that PSF is changing with time (thus requiring a new application of the new PSF even if the image it is operating on has remained the same). Although direct convolution with a PSF would be more computationally efficient under certain circumstances, the current implementation supports only convolution through multiplication in the fourier domain. Thus it is rather the fourier transform of the PSF, that is the optical transfer function (OTF), that is stored. This function multiplies the complex spatial spectrum of the image found using a FFT, followed by an inverse FFT operation to obtain the result. Therefore for a given OTF to be applied, the input image must be of a particular resolution in each of the spatial dimensions (which are always powers of 2) and with a particular pixel scale. Using input images which are not of that specified resolution requires that they first are zero-padded.

Furthermore, applying a pre-computed OTF to an image not having the specified pixel scale will first require resampling the image to match that pixel scale. However the preferred method when handling a series of images that will have a particular pixel scale is for the OTF to be set up for those particular images, avoiding this further repeated operation when processing new images. That can be done in the setup stage, in which a "sample image" is supplied to a function which sets up the OTF for each image plane. The setup program gathers from the sample image information concerning the effective wavelength of each image plane, and then creates for each image plane an OTF based on the PSF applying to that wavelength, and scaled according to the pixel scale of that sample image. Then the structure containing **N** OTF's is prepared to be directly applied to the fourier transform of each plane of an image having the same structure as that sample image.

Other modules require resampling the image in order to model spatial shifts, resampling in order to simulate rotations in the coordinate system, or resampling of the image at various points in order to modify the image resolution. Note that all resampling operations must assume that the image has been sufficiently band-limited (in the spatial domain) so that the resampling (implemented as a sinc interpolation filter) will not generate image artifacts due to aliasing. Thus a low-pass filter may be required prior to downsampling.

A few more of these image-affecting operations may be implemented within the camera/spectrometer functionalities (sect. 2.3.4), however these are not considered part of the imaging track since they are dependent on the modelling of one or another camera or spectrometer we have chosen to simulate (or multiple sets of these when more than one camera/spectrometer is active at one time, as will often be the case).

2.3.2 Throughput Track

The throughput track employs a structure which is setup to describe each of the (partially) transmissive elements in the optical train. This structure also describes the emissivity and temperature of (thus the thermal emission expected from) each of these optical elements, so this structure is also directly used by the background track (below). In addition to actual transmission coefficients, this structure may also be used to describe changes in units or representation. For instance, one element simply involves multiplication by the useful area of the E-ELT primary mirror, in order to convert units from spectral flux (in Janskys) to spectral power (in $10^{-26}W/Hz$).

As with setting up the OTF governing a convolution (as discussed above), it is possible for the throughput structure to be set up a single time and applied as needed. However in many other simulations there will be a change in the throughput during an observation (for instance, with the atmosphere when the zenith angle changes), or there will be a change only in the emission (due to a change in temperature). This can generally be accomplished by setting up the structure and later modifying a particular element to describe that change, after which the modified structure will be applied to new images, or to recompute the result using the modified throughput even with the input image unchanged.

Recall that each image structure consists both of the image information contained in **N** planes each describing a $\mathbf{J} \times \mathbf{K}$ image corresponding to a color, and a series of **N** spectra in N-chrome (or monochrome) mode. In imagecube mode, there are no spectra but there is instead an array of **N** scaling values (starting as an array of 1's) which affects the amplitude of each image plane similarly and which plays the same role as the **N** spectra for the purposes of the present discussion. This separation of the spatial and spectral components of the image means that the throughput track *does not affect the image planes at all, and is only applied to the spectral description* (as opposed to the imaging track which only affects the image planes and ignores the spectral information). Therefore, the throughput track is totally ignorant of the image-affecting operations discussed in sect. 2.3.1, and visa-versa. This allows each to be run independently, and on an as-needed basis. The throughput is applied by multiplying each of the **N** spectra, at each wavelength, by the transmission specified for each element in the throughput structure that has been set up.

The throughput structure currently includes the following elements:

- Atmospheric transmission
- The (imperfect) reflection due to the E-ELT optics, modelled collectively
- The input window of the METIS instrument
- The first dichroic, diverting the shorter wavelengths for use by the AO sensing camera
- The cold calibration unit (Dicke switch) which normally has a transmission of unity, but whose transmission is switched to zero when that unit is inserted
- The fore optics and derotator, consisting of 9 reflections modelled collectively
- The effective area of the telescope objective, resulting in a change of units

An additional throughput structure may be setup within the camera/spectrometer functionalities (sect. 2.3.4), however these are not considered part of the throughput track since they are dependent on the modelling of one or another camera or spectrometer we have chosen to simulate (or multiple sets of these when more than one camera/spectrometer is active at one time, as will often be the case). Notably, the second dichroic (separating the L-M and N bands, when used), the scaling from power to photon counts, and the detector quantum efficiency, are all implemented within these additional throughput structures used within each camera or spectrometer, but applied as described above.

2.3.3 Background Track

The background track uses the same throughput structure described above, but in order to apply the black-body emissions which are included therein. In doing so, the non-unity transmission of element **n** must be applied to the background as computed up to the output of element **n-1**; these transmission coefficients are contained in the same structure.

In addition to the **N** spectra attached to an image (in N-chrome mode) there is an additional spectrum describing the net background radiation. This is accumulated by processing the throughput structure, beginning with a background spectrum filled with 0's. Running through each element of the throughput structure (which are in the actual order of the elements in the optical train), the current background spectrum (at each wavelength) is multiplied by the throughput of that element, and then the emission from that element (if any) is added to the spectrum. That emission may be computed using the emissivity (1 - transmission) of the element and the modelled temperature of that element using the Planck black body radiation function. This calculation is omitted for elements with a modelled temperature of less than 80^o K (thus including all of the cold optics) which are considered to have negligible emission. Thus only the first 3 of the elements listed in sect. 2.3.2 contribute to the emission (but of course the non-unity transmission of all subsequent elements are taken into account).

Unlike the image information, the background emission is always reckoned in terms of $Jy/arcsec^2$ regardless of resampling which changes the size of pixels. The camera/spectrometer functionality (sect. 2.3.4) is responsible for integrating the background radiation presented to it with the image power, after multiplying the resulting background (in $Jy/arcsec^2$) by the telescope aperture area and the area of a detector pixel. Within the camera functionality the background spectrum may have been affected by transmissions described by an additional throughput structure, but this entails no added emission since these modelled components are at cold temperatures.

2.3.4 Camera and Spectrometer Functionality

The camera and/or spectrometer in use is the most flexible, and potentially the most complicated component of METIS to be simulated. Unlike the imaging track which only acts on the contents of the image planes, or the throughput and background tracks which only operate on the spectra attached to the image structures, the modules implementing the cameras and spectrometers generally operate on a non-trivial combination of both the image arrays and the spectra. In the most general terms, one could say that for each image pixel on each color plane, one of these modules will map its amplitude to a number of detector pixels in various proportions. Rather than the input which specifies the spectral power in that pixel (for that color plane), the output of this stage will be expressed in units of *detectable photons per second per detector pixel*.

That conversion first involves a multiplication of the spectral power by the integrated spectrum applicable to that image plane, thus having units of bandwidth. This is not truly an "effective bandwidth" since the spectrum itself is but a spectrally described scaling of the image; only if the spectrum had been of unity amplitude would the area under that curve describe the actual bandwidth of the color represented. Secondly, there is also a conversion from energy to photons (division by $h\nu$) and a further multiplication by the quantum efficiency of the illuminated detector for the wavelength(s) considered. The conversion to photons must be done right at this stage since the output of a camera module no longer contains wavelength information but is a single image plane (per detector array). Nor could the quantum efficiency have been applied earlier, since the same wavelength would obtain a different quantum efficiency from the different detectors in use.

Since more than one detector is often in use at the same time, this stage of the processing will generally involve running more than one module in parallel. In some cases there will be an additional division between the cameras simulated in order to take into account a mask at the entrance focal plane or, for instance, the field separation involved when the IFU obtains the central portion of the incoming image for spectroscopic analysis while allowing the peripheral image to proceed to the imaging camera(s). There will be a number of complications in the setup and implementation of the more complex modes of METIS such as coronography and polarimetry (polarimetry is not supported by the current image data structures which do not include polarimetric data). However even the more complex spectroscopic modes (particularly the IFU spectrograph) can be implemented within the architecture here described, as long as the hardware can be described in terms of the throughput from a given image pixel at a given wavelength to one or more detector pixels.

Currently only the straight imaging cameras have been implemented in code, and indeed this requires particularly simple code in relation to the general capabilities of these modules as described above. For in the case of the cameras, there is no detailed interaction between image position and wavelength, and the modelling only requires resampling onto the detector pixels and application of a throughput structure as described above (the cold optics of the camera generate no additional background emission to take into account). Additionally the step of mapping the input image pixels onto the detector pixels involves stepping through each of the **N** color planes but sending the resampled output to the *single* image plane describing the output of the camera module (again, in detectable photons per second per pixel), and for each input color plane the result on the output image is accumulated. Prior to that accumulation, a "throughput" has been applied (using the same tools as described in sect. 2.3.2) which has converted the power represented by that color plane into a rate of detectable photons, so no further scaling need be applied. This rather simple implementation of the imaging cameras is possible given that their optics produce (to first order) an undistorted copy of the input image with no chromatic aberration (the cameras focus using only reflective optics) and a spectral throughput (and conversion to detectable photons) that is independent of image position.

With the spectrometric modes, a much more complicated mapping will be required. This could be implemented through an algorithm which directly simulates the optics including the dispersive elements in detail. An alternative implementation essentially involves initially setting up a huge (but sparse) matrix which maps each input pixel to each output pixel with a given amplitude. The size of such a matrix would typically be extremely large (larger than the memory capacity of a modern PC!), but its non-zero elements could be reasonably stored given a suitable data representation. The advantage of the latter approach is that the (virtual) matrix multiplication could be computed much faster for a large number of varying input images, when that is part of the goal. For simulations in which only the detector action is repeatedly simulated (but using an incoming image which is unchanging), there is no advantage at all since setting up the (sparse) matrix requires essentially the same computations that are carried out in the first method employing an algorithm which models the optical hardware in detail.

In the coming months, the operation of both the long-slit spectroscope and the IFU imaging spectroscope will be coded using the framework we have described. Currently we have modelled the L-M band camera using the direct approach discussed above. The throughput structure employed in the camera stage includes the following elements:

- The second dichroic which reflects the shorter wavelength (L and M band) radiation toward this camera (so that an N band image could be obtained simultaneously using the light that proceeds toward the long wavelength camera)
- A spectral filter which may have been selected to pass the entire L (and/or M) band or only a small portion thereof
- A factor representing the (small) loss due to the camera optics
- The conversion from energy to photons, as discussed above
- The quantum efficiency of the HAWAII detector array

A more realistic simulation of the cameras could take into account the small amount of image distortion or misfocusing over the field due to the camera optics. This would still be independent of wavelength, and thus a less complicated module than will be required for implementing the spectroscopic modes.

2.3.5 Detectors

The final step of instrument simulation models the behaviour of the 3 detector systems which are illuminated according to the output images supplied by the camera modules. The basic function of the detector simulation is simple. Since the camera module has supplied an image in terms of "detectable photons per second" (thus taking into account the quantum efficiency of the following detector for the stream of photons of different wavelengths), which is geometrically matched to the detector pixels, the *mean* photocurrent generated within each detector

pixel is directly specified: one electron of current for each "detectable photon." An ideal detector would then produce a current integrated over the detector integration time (DIT) (thus *charge*) given by a Poisson random variable with that mean. Since any reasonable detector integration period will accumulate a charge of *much* more than 10 electrons, it is reasonable to approximate this random variable as the *exact* charge given by multiplying the mean photocurrent by the DIT, plus a noise term modelled as a zero-mean gaussian random variable with a variance (square of the standard deviation) given by that same number.

To model a practical detector, one must first add to the true photocurrent the dark current of the detector, and increase the variance of the noise process by (the square of) the readout noise for that detector system (which should therefore include contributions from the electronic pre-amp and analog-to-digital converter). These effects are included in the current software. Additionally one could model static detector effects such as variation in detector sensitivity as a function of pixel position and offset of the readout voltage as a function of pixel position, effects that would normally (and transparently) be eliminated in an early stage of the readout system using flat-field corrections. Properly modelling the rms noise for a practical detector could take into account nonuniform readout noise characteristics, or an "excess noise" figure (but probably not for the types of detectors whose use are anticipated). One could also model artifacts such as electronic noise sources (characterized either as white noise with an independent value each readout frame, or colored noise with respect to readout time according to a power spectrum) which are common to detector rows, columns, readout groups, or all pixels. There could also be (static) nonlinearities in the response of detector readouts, or crosstalk between detector pixels. Modelling such effects would be useful in generating data streams for testing the early stages of the detection system processing, but might not ever be needed for evaluating the astronomical performance of the instrument insofar as these effects can be removed in pre-processing or will have no significant net effect in the final reconstruction of an image or spectrum.

One other specification of a detector chip which deserves mention and which the simulator is aware of is the full well depth of the detector pixels. When using a longer DIT, it is possible for the charge in a pixel to approach this value at which point a predictable non-linearity sets in, with the further accumulation of charge at a rate of less than one electron per detectable photon, eventually falling to zero. This is crudely modelled in the current software as a hard limit at which point the gain goes from one to zero. Of greater usefulness, however, is the simulator's use of the full well charge to inform a user of the maximum advisable DIT according to the photocurrent predicted using the rest of the simulation. This maximum exposure would also be the ideal recommended exposure time to use (especially for the N band detector) since shorter exposures would accentuate the effect of detector readout noise. The simulator looks at the pixel with the largest predicted photocurrent, and divides this into the full well charge (reduced by a safety margin) to report to the user planning an observation the optimum DIT to use for that detector during the proposed observation.

The current METIS design includes two sorts of detector technology for the science detectors with widely different characteristics. A 2048×2048 pixel Teledyne HAWAII-II (HgCdTe) detector chip is used in the L-M band imager[‡], and four of these chips are used in the L-M band IFU spectrometer in order to include enough pixels for that function. The N band imager employs a 1024×1024 pixel Raytheon AQUARIUS (Si:As) chip. The expected characteristics of these devices (with the quantum efficiency at mid-band reported, whereas the simulator may employ a more detailed description of that parameter over wavelength) are summarized in Tab. 1.

2.3.6 Control program

All of the functional modules required for simulation of the entire E-ELT and METIS hardware have been included in the above sections 2.3.1 - 2.3.5. Each routine described is controlled only by input data and parameters passed to it (however many parameters are currently hard-coded which can in the future be supplied in the function call) by a higher level program. For proper modularity, the functions do not maintain any static memory of their own, but where such memory may be desired the outer program keeps track of these variables and returns them to the module at each call. Likewise the functions return results only to the calling program. For efficiency, most of these data (especially ones involving arrays) are actually referred to using pointers with the actual data stored in heap space.

[‡]The L-M band and N band imagers referred to are also the camera and detector systems used for long-slit spectroscopy, polarimetry, and coronography, with the insertion of appropriate optical elements.

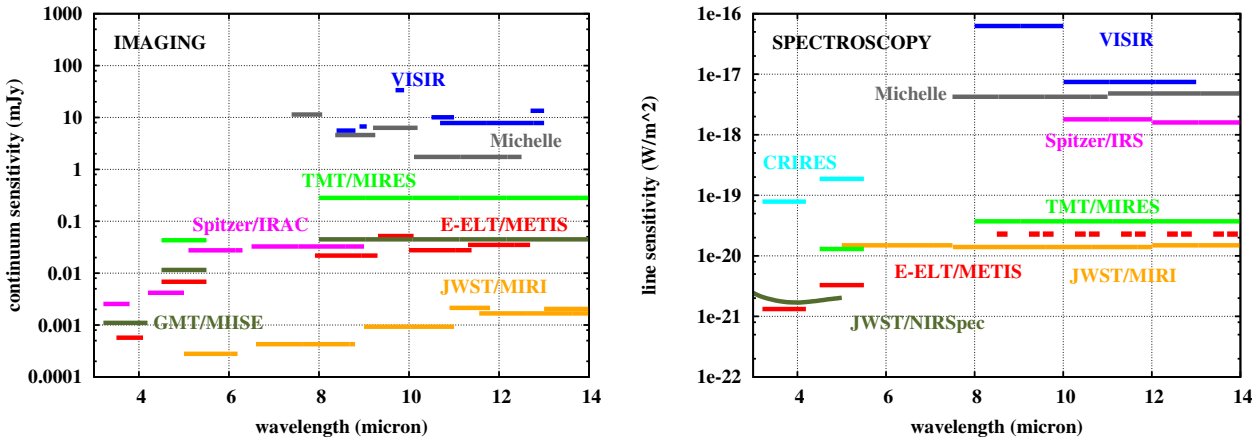

Figure 3. Sensitivity of the IFU-spectrograph and imager of METIS compared to other current and future instruments. Sensitivities are given for a one hour exposure of a point source with 20% overhead and a signal-to-noise of 10σ. The calculations of these sensitivities are based on an earlier version of the simulator developed by Sarah Kendrew.[8]

Therefore there must be one outer program which integrates all of the simulator functions through calling the modules at appropriate times and passing data in between them. In addition to managing the flow of these data, the outer program determines the order in which modules are called (so that a module is called only after its input data are available) and the times at which a module is again run, either to account for a change in its input data, or to generate a new realization of a random process (particularly in order to simulate repeated detector exposures, but also in the case of any other module with a stochastic component). In its current early stage, the outer program to implement a particular simulation is written on an *ad hoc* basis, following a basic template. In the future, it is anticipated that there will be a single control program (or perhaps a few different ones for widely different sorts of simulations) where its specific behaviour (in terms of data representations and simulated timing) and assumed parameters are governed by a set of ASCII configuration files submitted by a user. The outer program will also direct the output of the simulator into FITS files describing the simulated detector readout frames for use by the user, to be fed into the eventual data reduction software to be employed for the METIS instrument.

3. RESULTS

3.1 Sensitivity of METIS compared to current and future facilities

Performance calculations were already realized with an earlier version of the simulator developed by Kendrew et al.[8] This simulator calculates the performance of METIS, including the effects of the atmospheric turbulence, i.e. the adaptive optics performance, the thermal background originating from the sky, telescope and instrument, and the expected detector performance, as well as the instrumental, telescope and atmospheric throughput. The calculations were updated for this paper with the current telescope and detector parameters. The underlying parameters are identical with those used for the new simulator presented in this paper, see Table 1. We are assuming the best case of a point source and unresolved spectral lines for the sensitivity calculations.
The sensitivities originating from these calculations are compared to the performance of other current or future space- and ground-based instruments operating in the mid-infrared wavelength regime. The sensitivity values of these instruments were taken from literature and then scaled to a detection of an unresolved point source with a signal-to-noise of 10σ in an 1-hour observation including 20% overhead. The spectroscopic sensitivities should be taken with care, given the different resolving powers of the individual instruments. The plots showing the performance comparison for the imaging and IFU high-resolution spectroscopy observing modes are shown in Fig. 3.

For imaging the performance of METIS is compared to that of the current instruments IRAC[9] on board the Spitzer Space Telescope, VISIR[10] at the VLT, and Michelle[11] at Gemini-N. Additional the expected performance

of three contemporary instruments, MIISE[12] at the Giant Magellan Telescope, MIRES[13] at the Thirty Meter Telescope (TMT) and MIRI[14] on board the JWST are shown. The performance of MIRI will be updated from the expected ones with the recently, during the instrumental performance tests measured, ones, as soon as they are published.
As shown in Fig. 3, left, only JWST/MIRI's imaging performance is expected to be substantially better than that of METIS, offering a continuous coverage of the mid-IR wavelength regime, but with a much lower spatial resolution. Therefore MIRI and METIS will provide excellent complementary observations.

For spectroscopy the line sensitivities of METIS are compared to VISIR, Michelle, MIRES and MIRI, as for the imager, and additional with CRIRES[15] at the VLT, the Infrared Spectrograph IRS[16] on board Spitzer, and NIRSpec[§], which will fly on board JWST.
Most comparable to METIS in terms of wavelength coverage and spectral resolution is CRIRES. As can be seen in Fig. 3, right, METIS will offer an substantially improvement in line sensitivity compared to CRIRES of an order of one to two magnitudes. Furthermore, METIS will offer the only high-resolution 3D spectrograph in the mid-infrared wavelength regime in the next decade.

3.2 Imaging simulations

Up to now, only the imaging arm of the simulator has been implemented in code. First simulations of an observation of a high-redshift galaxy have been performed. Details of the setup of these simulations and images showing the input file and the simulated output file are presented in another paper of these proceedings by Brandl et al.[5] (2012, paper 8446-57).

4. SUMMARY AND OUTLOOK

We have presented in this paper the development of the end-to-end simulator for the coming mid-infrared E-ELT instrument METIS. Currently we have modeled the L-M band camera and are ready to generate detector data in straight imaging mode. First simulations have been performed of a high- redshift galaxy (presented in[5]). The simulator structure consists of separated modules, each with a well defined input, output and range of behaviours, described in detail in Sect. 2.3. The simulator can be fed by any kind of science image in FITS format, including a specific set of keywords to describe the data, and produces a detector image also in FITS format, suitable for further analysis with already existing data reduction software and/or the in the future to be developed data reduction pipeline of METIS. This simple way of providing input files makes the simulator very powerful and useful for the science community.
In the coming months, the operation of both the long-slit spectroscope and the IFU imaging spectroscope will be coded using the framework we have described.

REFERENCES

[1] Brandl, B. R., Lenzen, R., Pantin, E., Glasse, A., Blommaert, J., Venema, L., Molster, F., Siebenmorgen, R., Kendrew, S., Baes, M., Böhnhardt, H., Brandner, W., van Dishoeck, E., Henning, T., Käufl, H. U., Lagage, P.-O., Moore, T. J. T., Waelkens, C., and van der Werf, P., "Instrument concept and science case for the mid-IR E-ELT imager and spectrograph METIS," *Proc. SPIE* **7735** (2010).

[2] Delabre, B., "39 m ELT optical design report," tech. rep. (2011).

[3] Davies, R., Ageorges, N., Barl, L., Bedin, L. R., Bender, R., Bernardi, P., Chapron, F., Clenet, Y., Deep, A., Deul, E., Drost, M., Eisenhauer, F., Falomo, R., Fiorentino, G., Förster Schreiber, N. M., Gendron, E., Genzel, R., Gratadour, D., Greggio, L., Grupp, F., Held, E., Herbst, T., Hess, H.-J., Hubert, Z., Jahnke, K., Kuijken, K., Lutz, D., Magrin, D., Muschielok, B., Navarro, R., Noyola, E., Paumard, T., Piotto, G., Ragazzoni, R., Renzini, A., Rousset, G., Rix, H.-W., Saglia, R., Tacconi, L., Thiel, M., Tolstoy, E., Trippe, S., Tromp, N., Valentijn, E. A., Verdoes Kleijn, G., and Wegner, M., "MICADO: the E-ELT adaptive optics imaging camera," *Proc. SPIE* **7735** (2010).

[§]http://www.stsci.edu/jwst/instruments/nirspec/sensitivity/

[4] Thatte, N., Tecza, M., Clarke, F., Davies, R. L., Remillieux, A., Bacon, R., Lunney, D., Arribas, S., Mediavilla, E., Gago, F., Bezawada, N., Ferruit, P., Fragoso, A., Freeman, D., Fuentes, J., Fusco, T., Gallie, A., Garcia, A., Goodsall, T., Gracia, F., Jarno, A., Kosmalski, J., Lynn, J., McLay, S., Montgomery, D., Pecontal, A., Schnetler, H., Smith, H., Sosa, D., Battaglia, G., Bowles, N., Colina, L., Emsellem, E., Garcia-Perez, A., Gladysz, S., Hook, I., Irwin, P., Jarvis, M., Kennicutt, R., Levan, A., Longmore, A., Magorrian, J., McCaughrean, M., Origlia, L., Rebolo, R., Rigopoulou, D., Ryan, S., Swinbank, M., Tanvir, N., Tolstoy, E., and Verma, A., "HARMONI: a single-field wide-band integral-field spectrograph for the European ELT," *Proc. SPIE* **7735** (2010).

[5] Brandl, B. R., Lenzen, R., Pantin, E., Glasse, A., Blommaert, J., Meyer, M., Guedel, M., Venema, L., Molster, F., Stuik, R., Schmalzl, E., Meisner, J., Le Floc'h, E., Brandner, W., Hippler, S., Snellen, I., Pontoppidan, K., and the METIS team, "METIS: the thermal infrared instrument for the E-ELT," *Proc. SPIE* **8446** (2012).

[6] Wells, D. C., Greisen, E. W., and Harten, R. H., "*FITS - a Flexible Image Transport System*," *A&AS* **44**, 363–+ (1981).

[7] Schöck, M., Els, S., Riddle, R., Skidmore, W., Travouillon, T., Blum, R., Bustos, E., Chanan, G., Djorgovski, S. G., Gillett, P., Gregory, B., Nelson, J., Otárola, A., Seguel, J., Vasquez, J., Walker, A., Walker, D., and Wang, L., "Thirty Meter Telescope Site Testing I: Overview," *PASP* **121**, 384–395 (Apr. 2009).

[8] Kendrew, S., Jolissaint, L., Brandl, B., Lenzen, R., Pantin, E., Glasse, A., Blommaert, J., Venema, L., Siebenmorgen, R., and Molster, F., "Mid-infrared astronomy with the E-ELT: performance of METIS," *Proc. SPIE* **7735** (2010).

[9] Fazio, G. G., Hora, J. L., Allen, L. E., Ashby, M. L. N., Barmby, P., Deutsch, L. K., Huang, J.-S., Kleiner, S., Marengo, M., Megeath, S. T., Melnick, G. J., Pahre, M. A., Patten, B. M., Polizotti, J., Smith, H. A., Taylor, R. S., Wang, Z., Willner, S. P., Hoffmann, W. F., Pipher, J. L., Forrest, W. J., McMurty, C. W., McCreight, C. R., McKelvey, M. E., McMurray, R. E., Koch, D. G., Moseley, S. H., Arendt, R. G., Mentzell, J. E., Marx, C. T., Losch, P., Mayman, P., Eichhorn, W., Krebs, D., Jhabvala, M., Gezari, D. Y., Fixsen, D. J., Flores, J., Shakoorzadeh, K., Jungo, R., Hakun, C., Workman, L., Karpati, G., Kichak, R., Whitley, R., Mann, S., Tollestrup, E. V., Eisenhardt, P., Stern, D., Gorjian, V., Bhattacharya, B., Carey, S., Nelson, B. O., Glaccum, W. J., Lacy, M., Lowrance, P. J., Laine, S., Reach, W. T., Stauffer, J. A., Surace, J. A., Wilson, G., Wright, E. L., Hoffman, A., Domingo, G., and Cohen, M., "The Infrared Array Camera (IRAC) for the Spitzer Space Telescope," *The Astrophysical Journal Supplement Series* **154**, 10–17 (2004).

[10] Lagage, P. O., Pel, J. W., Authier, M., Belorgey, J., Claret, A., Doucet, C., Dubreuil, D., Durand, G., Elswijk, E., Girardot, P., Käufl, H. U., Kroes, G., Lortholary, M., Lussignol, Y., Marchesi, M., Pantin, E., Peletier, R., Pirard, J.-F., Pragt, J., Rio, Y., Schoenmaker, T., Siebenmorgen, R., Silber, A., Smette, A., Sterzik, M., and Veyssiere, C., "Successful Commissioning of VISIR: The Mid-Infrared VLT Instrument," *The Messenger* **117**, 12–16 (Sept. 2004).

[11] Bryson, I. R., Glasse, A. C., and Atad-Ettedgui, E. I., "Michelle, mid-infrared spectrometer and imager," *Proc. SPIE* **2198** (1994).

[12] "Conseptual Design Review of GMT: MIISE (section 13.3)," (2006).

[13] "TMT Instrumentation and Performance Handbook," tech. rep. (2010).

[14] Swinyard, B. M., Rieke, G. H., Ressler, M., Glasse, A., Wright, G. S., Ferlet, M., and Wells, M., "Sensitivity estimates for the mid-infrared instrument (MIRI) on the JWST," *Proc. SPIE* **5487** (2004).

[15] Käufl, H.-U., Ballester, P., Biereichel, P., Delabre, B., Donaldson, R., Dorn, R., Fedrigo, E., Finger, G., Fischer, G., Franza, F., Gojak, D., Huster, G., Jung, Y., Lizon, J.-L., Mehrgan, L., Meyer, M., Moorwood, A., Pirard, J.-F., Paufique, J., Pozna, E., Siebenmorgen, R., Silber, A., Stegmeier, J., and Wegerer, S., "CRIRES: a high-resolution infrared spectrograph for ESO's VLT," *Proc. SPIE* **5492** (2004).

[16] Houck, J. R., Roellig, T. L., van Cleve, J., Forrest, W. J., Herter, T., Lawrence, C. R., Matthews, K., Reitsema, H. J., Soifer, B. T., Watson, D. M., Weedman, D., Huisjen, M., Troeltzsch, J., Barry, D. J., Bernard-Salas, J., Blacken, C. E., Brandl, B. R., Charmandaris, V., Devost, D., Gull, G. E., Hall, P., Henderson, C. P., Higdon, S. J. U., Pirger, B. E., Schoenwald, J., Sloan, G. C., Uchida, K. I., Appleton, P. N., Armus, L., Burgdorf, M. J., Fajardo-Acosta, S. B., Grillmair, C. J., Ingalls, J. G., Morris, P. W., and Teplitz, H. I., "The Infrared Spectrograph (IRS) on the Spitzer Space Telescope," *The Astrophysical Journal Supplement Series* **154**, 18–24 (2004).